

Supplementary Information

How the Ionic Liquid BMIMBF₄ influences the formation and optoelectronic properties of MAPbI₃ thin films

Simon Biberger¹, Konstantin Schötz¹, Philipp Ramming¹, Nico Leupold², Ralf Moos², Anna Köhler¹, Helen Grüninger,³ Fabian Panzer^{1*}

¹Experimental Physics II, University of Bayreuth, Bayreuth, Germany;

²Department of Functional Materials, University of Bayreuth, Bayreuth 95440, Germany;

³Northern Bavarian NMR Centre (NBNC) and Inorganic Chemistry, University of Bayreuth, Bayreuth, Germany.

Corresponding Author:

*E-Mail: fabian.panzer@uni-bayreuth.de

S1: Detailed description of the measurement setup

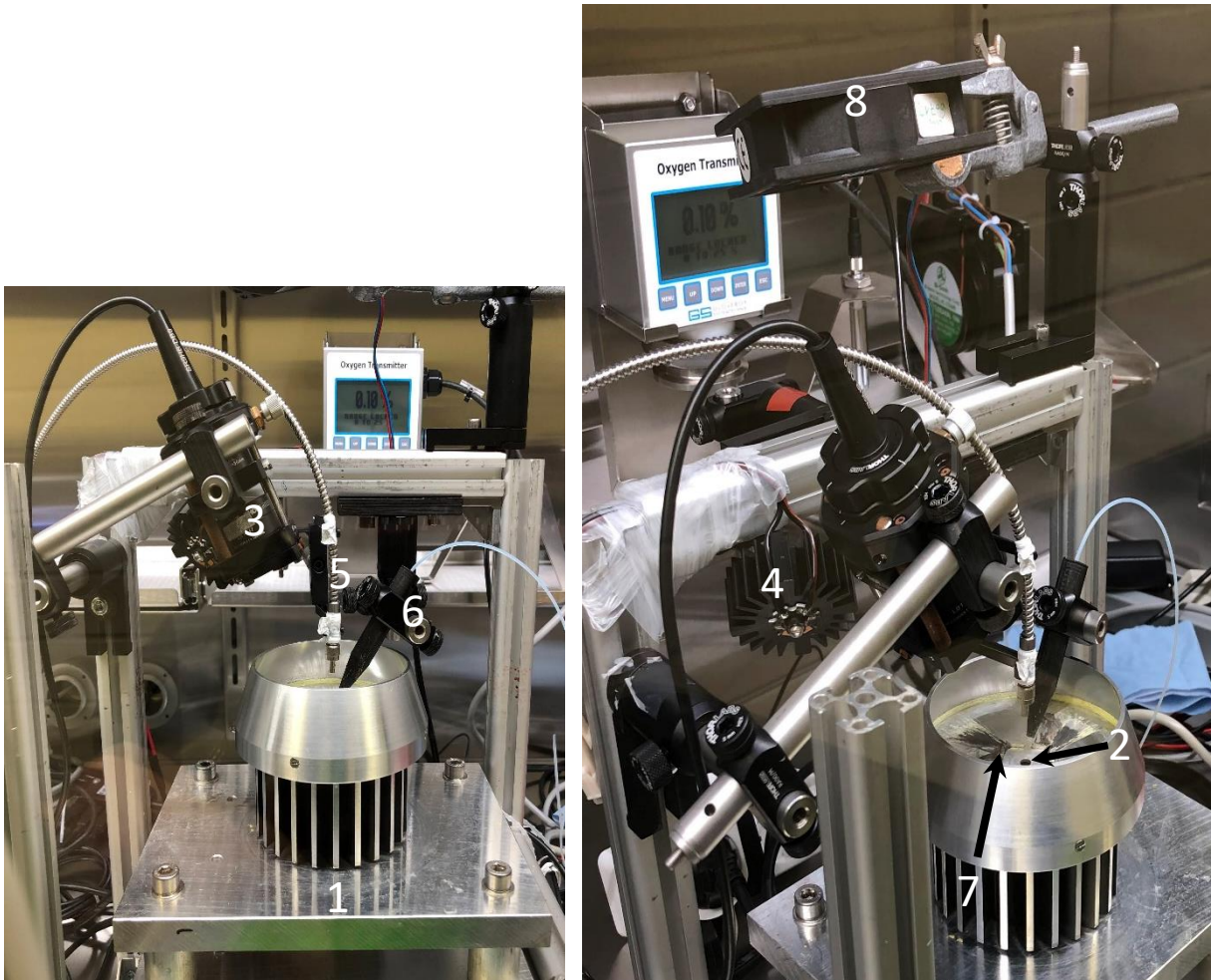


Fig. S1: Photographs of the setup used for measuring the in situ optical data during spin coating.

The setup for measuring the in situ optical data during spin-coating. It consists of a custom-built spin-coater (1) with a hole in the middle (2). Underneath the spin-coater a white-light LED is placed. Its light shines through the hole in the middle of the spin-coater and serves as a white light for transmission measurements. A laser diode (405 nm) in combination with focusing optics and a diaphragm (3) are mounted above the spin-coater for exciting the sample for PL measurements. An LED emitting at 490 nm (4) is placed next to the laser, whose scattered light can be detected (referred to as scatter-LED). The circular area probed by our optical measurements during the spin-coating has a diameter of 5 mm in the center of the substrate. White-light and excitation laser are turned on and off alternately, so that either transmission or PL is probed. Transmitted light, PL and scattered LED light are collected with one optical fiber (5),

which is coupled to the detection system. The detection system consists of a CCD camera, coupled to a spectrograph, and a home-built detection setup, which is described in detail in Supporting Reference 1. In brief, the detection setup switches the optical path between transmission and PL measurements, so that for PL measurements, the laser wavelength is blocked by a suitable filter. In contrast, for transmission measurements, the transmitted light is coupled into the spectrograph without additional filtering. The detection setup further synchronizes the CCD camera with the white-light LED, the laser and the optical path switching. Using this setup, we can record PL and transmission during spin-coating quasi-simultaneously (i.e., alternating frame by frame) with a rate of more than 10 Hz. From the transmission measurements, the optical density (OD) is calculated based on a reference measurement prior to spin-coating. Scattered LED light is recorded during the PL measurements. For experiments using the solvent engineering, the antisolvent can be applied via a syringe connected to a capillary (6). The substrate is physically held into place by barriers (7) to ensure the measurements during the processing are taken from the same sample area. To avoid a built-up of solvent atmosphere which can impact the film formation properties, a fan (8) is placed above the spin coater chuck.

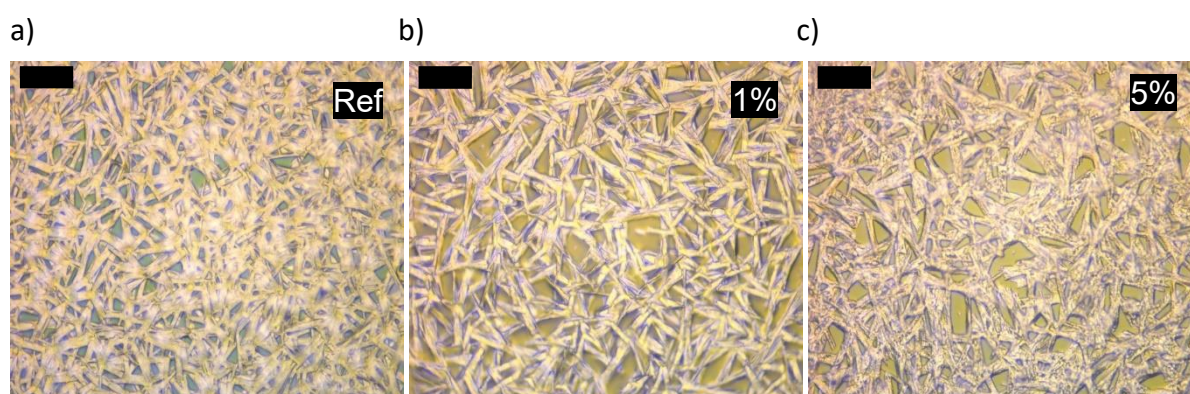


Fig. S2: Microscopy image of a) the reference film, b) the film with 1 mol% BMIMBF₄ and c) the film with 5 mol% BMIMBF₄ processed via one-step spin coating of MAPbI₃ in DMF at 2000 RPM. The scale bar is 20 μ m.

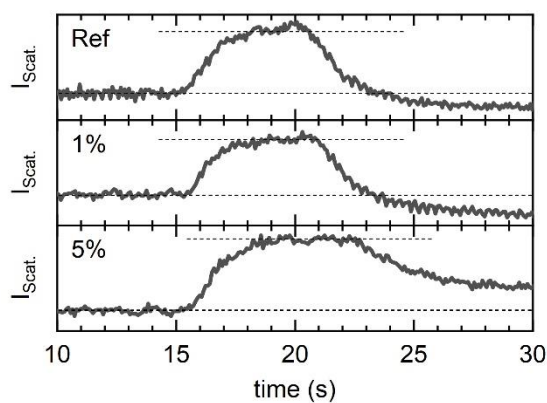


Fig. S3: Time evolution of the intensity of the scattered light during one-step spin coating at 2000 RPM of MAPbI₃ in DMF with different IL contents as indicated. The dashed lines indicate the initial intensity level and the high intensity level after solvent-complex formation.

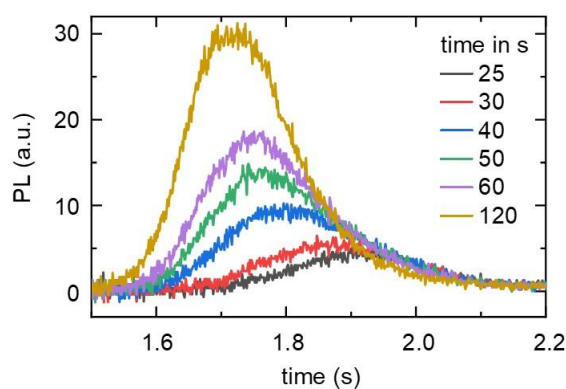


Fig S4: PL spectra at different times of the reference sample processed without IL via one-step spin coating at 2000 RPM of MAPbI₃ in DMF.

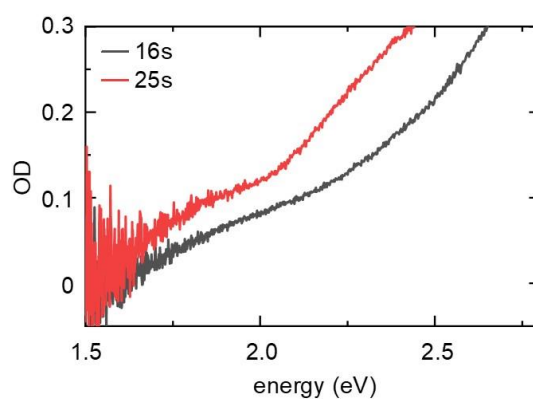


Fig. S5: Absorption spectra after 16 s (black) and 25 s (red) of the reference sample processed without IL via one-step spin coating at 2000 RPM.

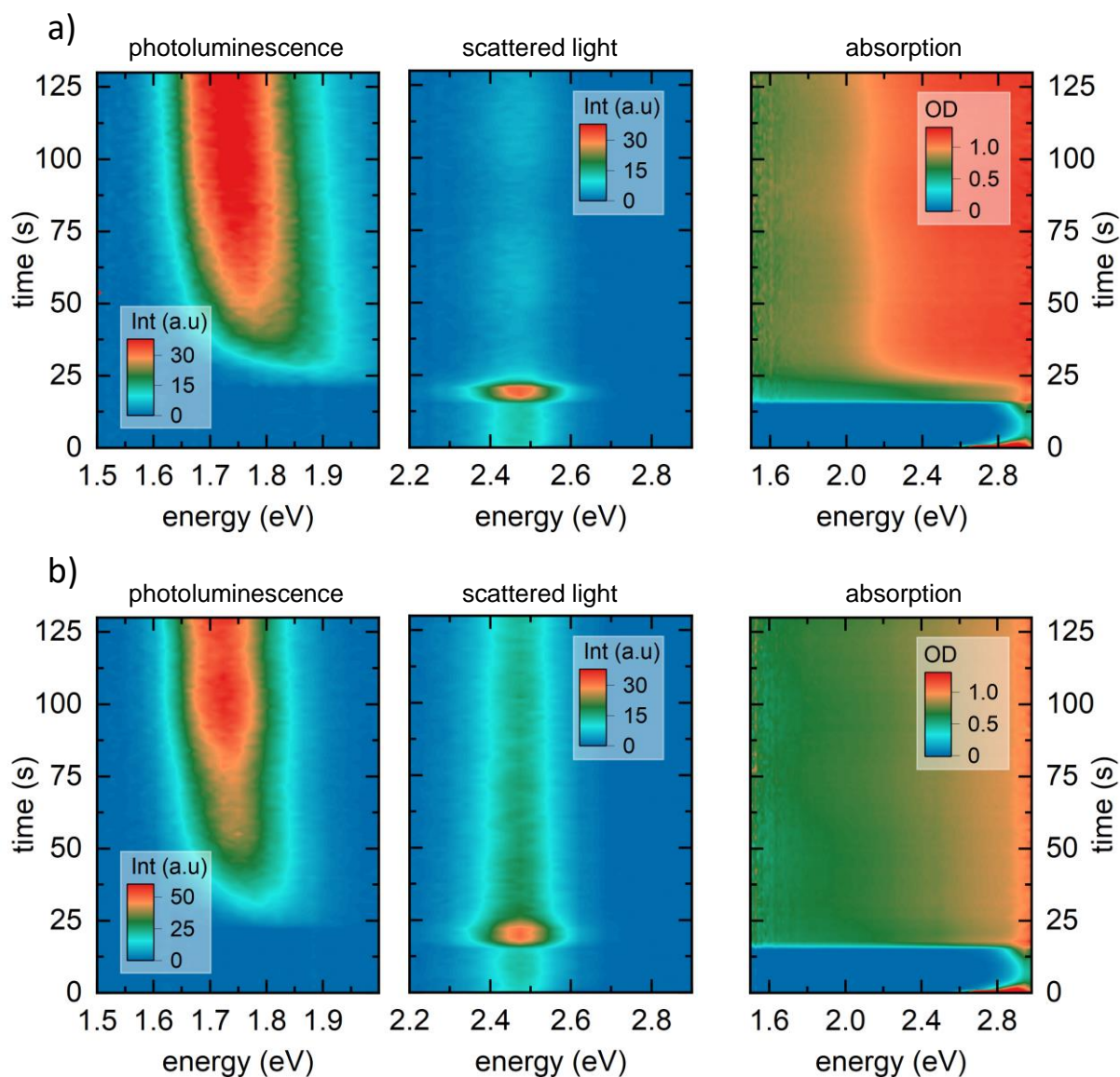


Fig. S6: Heat maps of photoluminescence (PL), scattered light, and optical density (OD) measurement during one-step spin coating at 2000 RPM of the solutions with a) 1 mol% BMIMBF₄ and b) 5 mol% BMIMBF₄.

S2: Estimation of layer thickness based on white light interference:

As described in our previous work¹, prior to the formation of the intermediate phase, we observe a sinusoidal modulation of the OD spectrum upon spin-coating (see Figure S7a). Such a modulation is indicative of positive and negative interference of white light caused by a thin layer and reflection at its interfaces. If the refractive index of the

layer causing the interference is known, the thickness of the layer can be calculated from the distance of adjacent extrema in the OD using^{2,3}

$$d = \frac{\lambda_1 \lambda_2}{2(n_2 \lambda_1 - n_1 \lambda_2)}, \quad (\text{S1})$$

where λ_i is the wavelength of the extremum i and n_i is the refractive index at wavelength λ_i . Assuming that n is roughly constant in the investigated spectral range, i.e. $n_1 \approx n_2$, and converting the wavelength to energy, Equation S1 can be re-written to

$$d = \frac{hc}{2n\Delta E}, \quad (\text{S2})$$

where ΔE is the energetic difference of two adjacent extrema in the OD. ΔE was extracted from the frequency of a sine function of the form

$$OD = \sin(\Delta E * (x + x_0)) + y_0 + m * x \quad (\text{S3})$$

fitted to the OD (see black dashed line in Figure S7a. The thickness of the layer was then calculated using the refractive index of DMF, that is $n = 1.43$. The calculated layer thickness using Equation S2 is shown in Figure S7b. Note that if the refractive index of the solution layer is higher than of pure DMF due to the presence of solute PbI_2 , the resulting layer thickness would be smaller. Thus, the layer thickness calculated with the refractive index of DMF can be seen as an upper limit to the actual layer thickness of the solution layer.

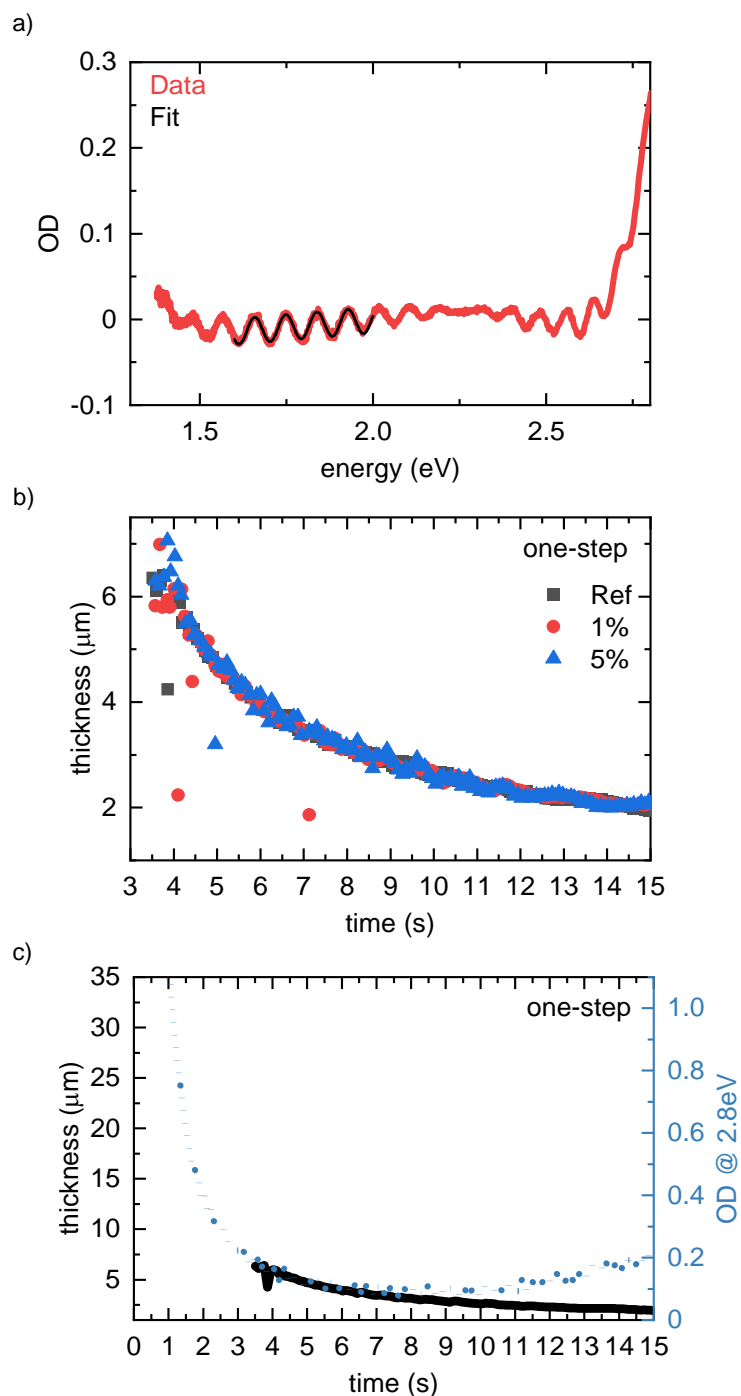


Fig. S7: a) Sinusoidal modulation of the measured OD spectrum caused by white light interference (red) together with a sine function following Equation S3, fitted to the measured OD (black) b) Time evolution of the solution layer thickness as extracted from the white light interference during one-step spin coating at 2000 rpm for precursor solutions containing different contents of BMIMBF₄. c) Evolution of the solution layer thickness of the reference precursor solution (black solid), together with the evolution of the OD at 2.8eV (blue dotted) within the first 15s of spin coating. Between 3.5s and 7s, both the solution layer thickness and the OD at 2.8eV follow the same qualitative decrease. While the solution layer thickness

continuously keeps decreasing after 7s, the OD at 2.8 eV stays constant until 9s, and increases afterwards. The fast decrease of OD and solution layer thickness in the first 7s indicates a throw-off of precursor solution, while between 7s and 9s the constant OD and continuous decrease of solution layer thickness suggest a mere evaporation of the solvent. The increase of OD from 9s onwards, while the solution layer thickness further decreases, can be associated to the change of the iodoplumbate precursor properties.

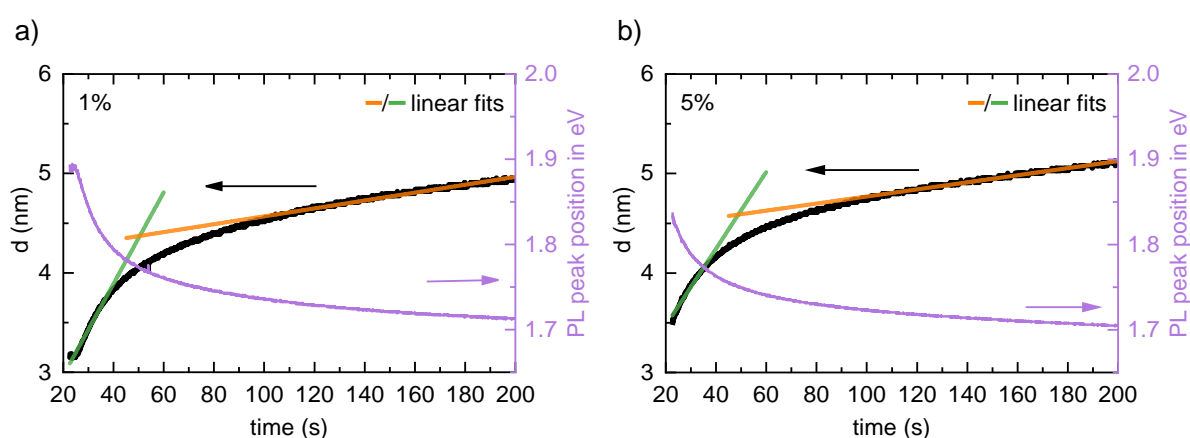


Fig. S8: Time evolution of the PL peak position (pink) and the resulting crystallite size (black), calculated via quantum confinement, for a) the solution with 1 mol% of IL and b) the solution with 5 mol% of IL. The green and orange lines show linear fits, from which the crystallite growth rates are extracted.

For fitting the PL spectra, we use an empirical line shape in the form of an asymmetric hyperbolic secant, that is

$$I(E) = I_0 \frac{2}{e^{\frac{E-E_0}{\sigma_1}} + e^{\frac{E-E_0}{\sigma_2}}} \quad (\text{S4})$$

S3: Aliasing effect and smoothing of the data

All signal intensities (transmitted white light, scattered LED light, PL) depend slightly on the angular position of the spin coater, i.e. the detectable intensities change with the frequency of the spin coater due to the rotation of the spin coater. Combined with the finite frequency of detection, this leads to aliasing when the Nyquist criterion cannot be met. As a result, the recorded signal is modulated with the aliasing frequency. Since the modulation is always much faster than the observed processes during film formation, the data can be corrected against this modulation. As reported in our earlier work,¹ this frequency can be filtered out by applying a notch filter in this frequency range or by using a Savitzky-Golay filter with a window size of 25 points and a polynomial order of 2. Both methods resulted in a similarly smooth curve. Therefore, we treated the data with a Savitzky-Golay filter when smoothing was indicated.

Additionally, the same smoothing method was applied to the PL spectra after 72 hours in Figure 4e due to a poor signal to noise ratio.

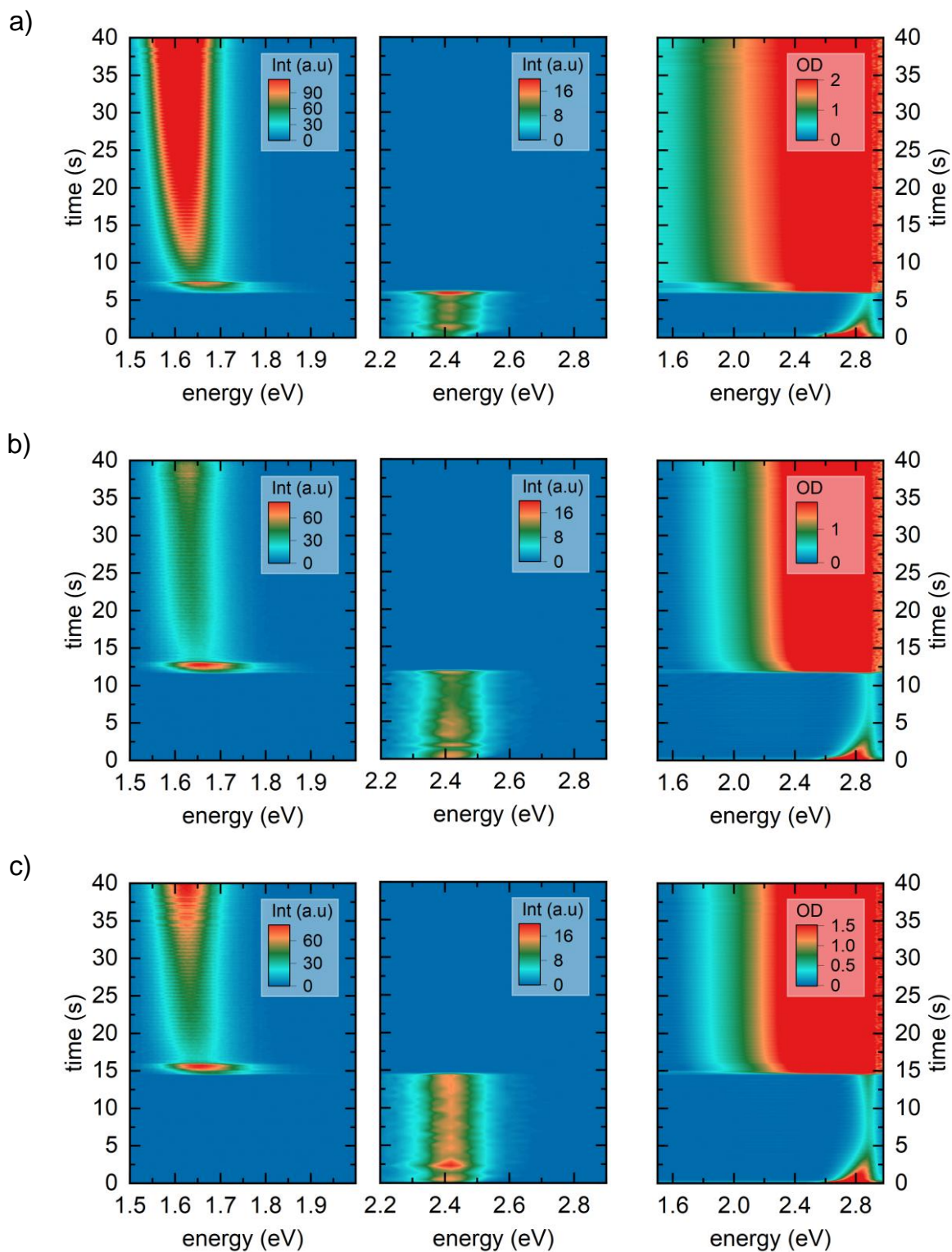


Fig. S9: Heat maps of photoluminescence (PL), scattered light, and optical density (OD) measurement at 2000 RPM of the reference solution without IL, processed via the solvent engineering approach. The antisolvent was dripped after a) 6 s, b) 12 s, and c) 15 s.

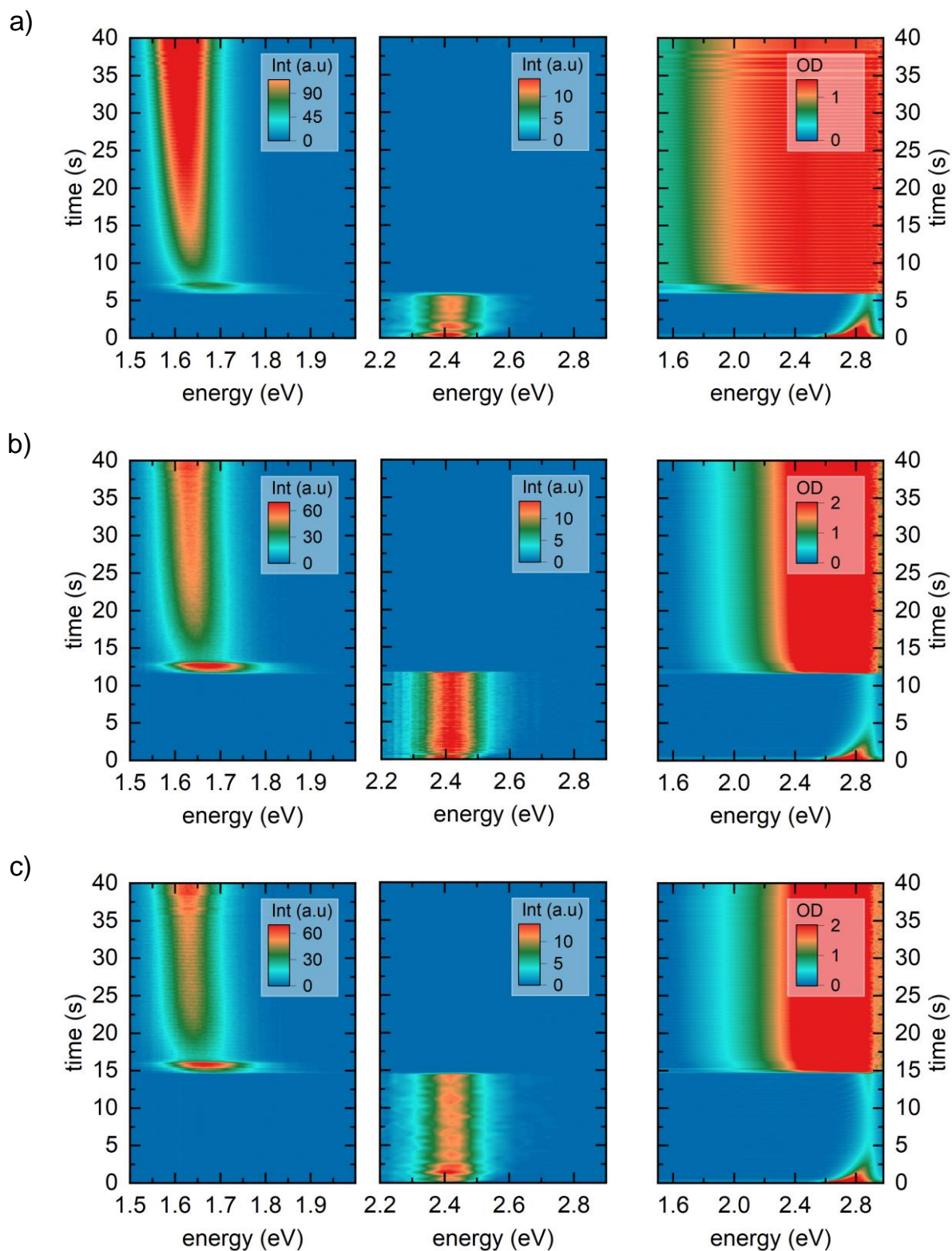


Fig. S10: Heat maps of photoluminescence (PL), scattered light, and optical density (OD) measurement at 2000 RPM of the solution with 1mol% BMIMBF₄, processed via the solvent engineering approach. The antisolvent was dripped after a) 6 s, b) 12 s, and c) 15 s.

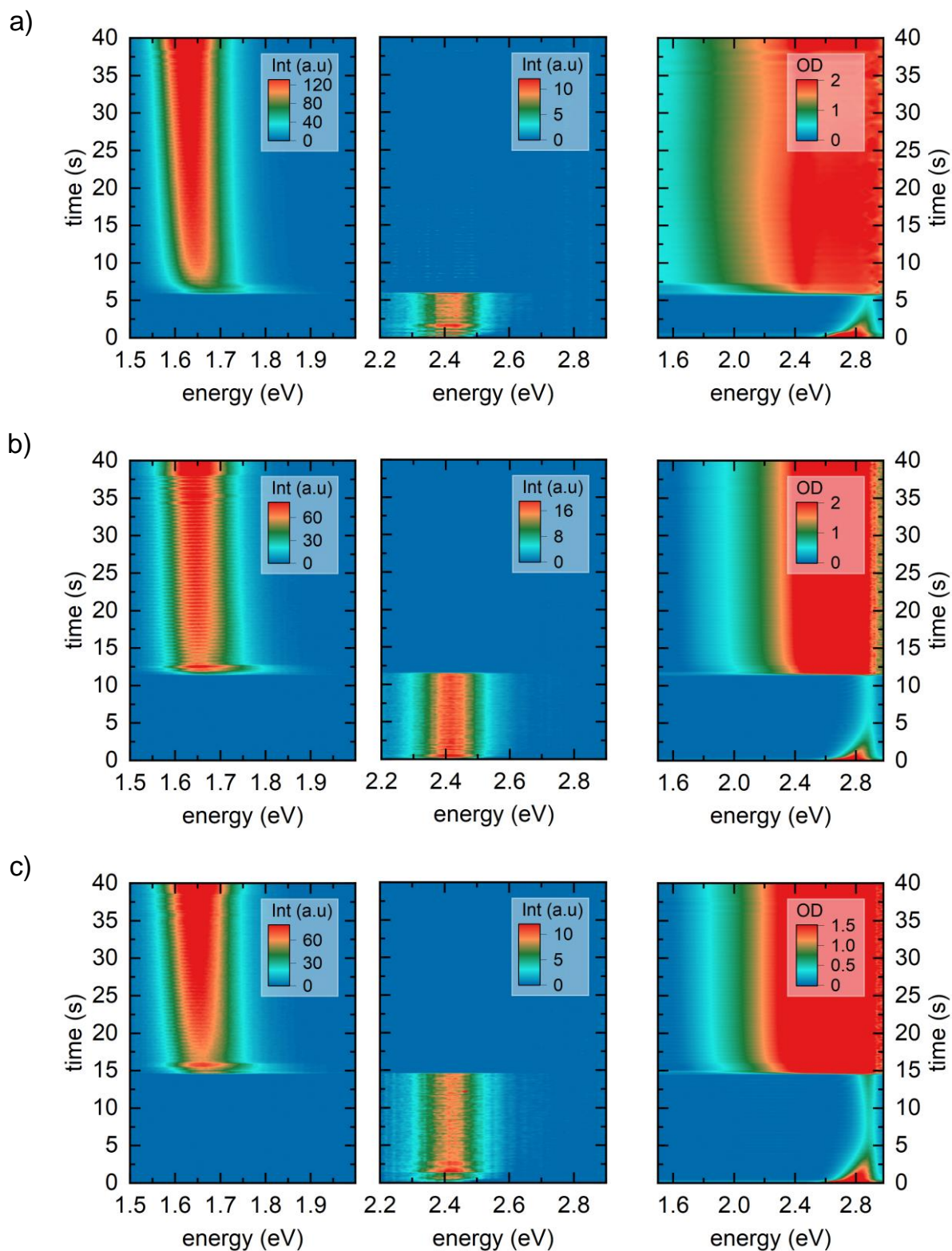


Fig. S11: Heat maps of photoluminescence (PL), scattered light, and optical density (OD) measurement at 2000 RPM of the solution with 5mol% BMIMBF₄, processed via the solvent engineering approach. The antisolvent was dripped after a) 6 s, b) 12 s, and c) 15 s.

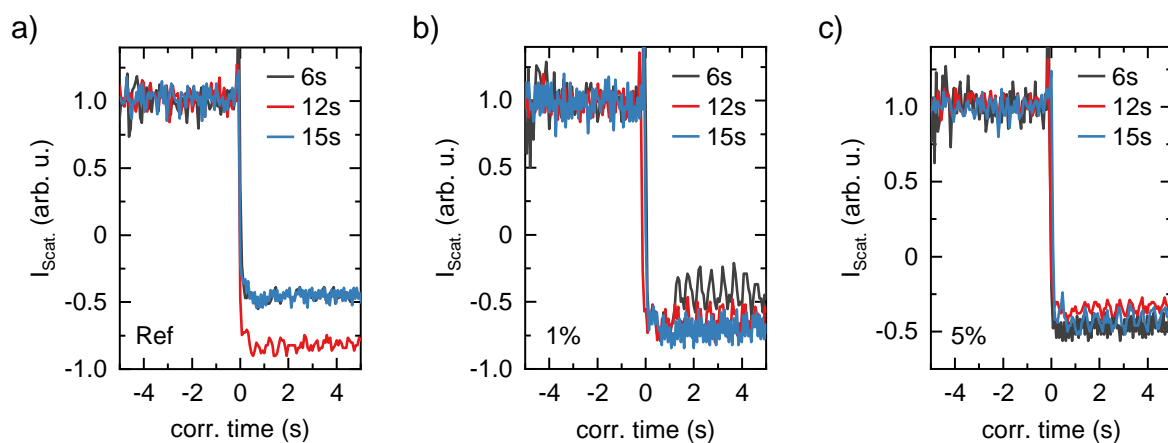


Fig. S12: Normalized temporal evolution of the intensity of the scattered light for different anti-solvent dripping time points for a) the samples without IL, b) the samples with 1 mol% of IL and c) the samples with 5 mol% of IL. $t = 0$ of the time axis is shifted to match the time of the AS dripping.

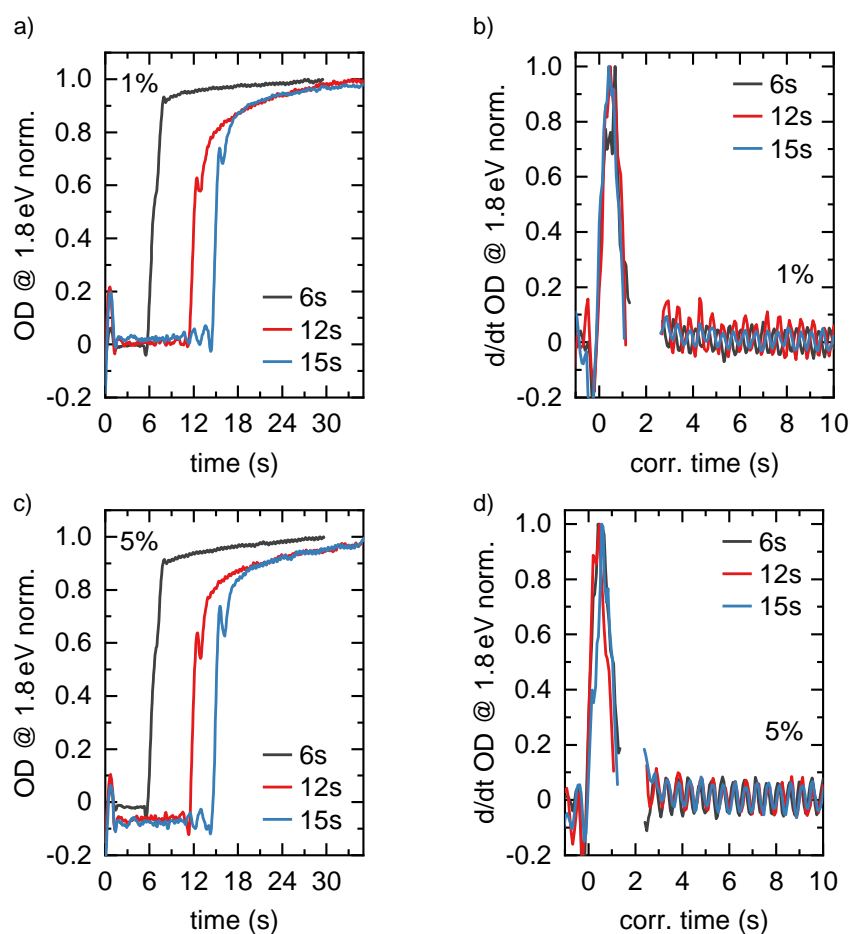


Fig S13: a) Time evolution of the OD at 1.8 eV for the 1mol% IL sample and for different anti-solvent dripping time points. b) normalized time derivative of the OD at 1.8 eV for the 1mol%

IL sample and for different AS dripping time points. $t = 0$ of the time axis is shifted to match the time of the AS dripping. c) Time evolution of the OD at 1.8 eV for the 5mol% IL sample and for different AS dripping time points. d) Normalized time derivative of the OD at 1.8 eV for the 5mol% IL sample and for different AS dripping time points. $t = 0$ of the time axis is shifted to match the time of the AS dripping

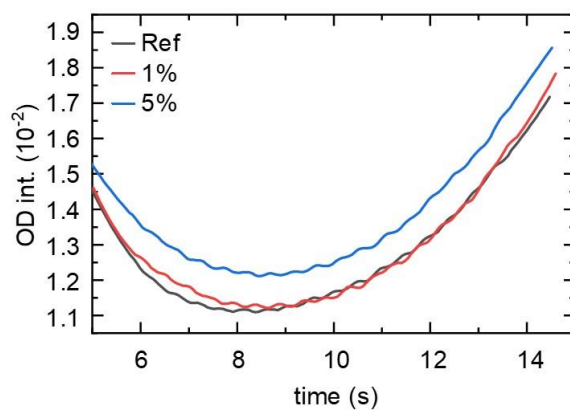


Fig S14: Time evolution of the OD, integrated between 2.84eV and 2.87eV, for precursor solutions, containing different amounts of IL as indicated.

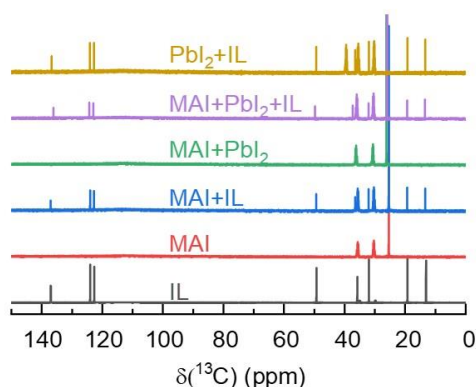


Fig S15: ^{13}C NMR spectra of the IL solution, the single precursor solutions with and without 5 mol% IL, and the MAPbI_3 solution with 5 mol% IL. The solvent for all precursor-solutions is DMF-d_7 . In case of PbI_2 a drop of DMSO-d_6 was further added to solve PbI_2 entirely.

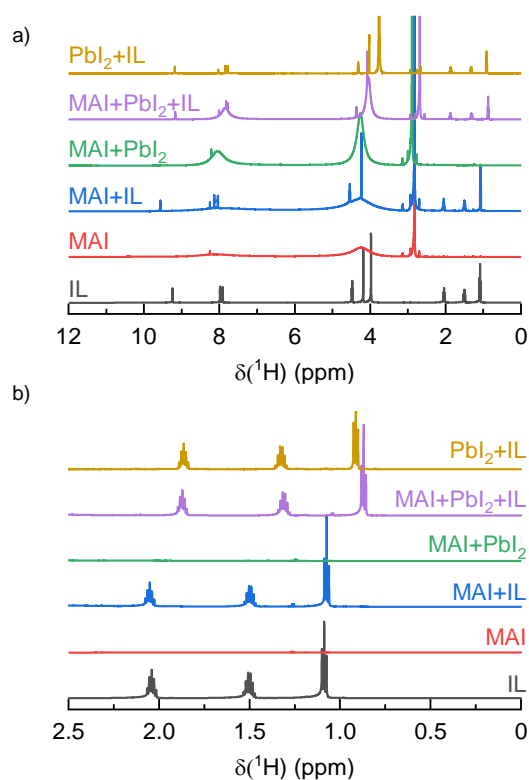


Fig S16: a) ^1H NMR spectra of the IL solution, the single precursor solutions with and without 5 mol% IL, and the MAPbI_3 solution with and without 5 mol% IL. The solvent for all precursor-solutions is DMF-d_7 . In case of PbI_2 a drop of DMSO-d_6 was further added to solve PbI_2 entirely. b) Enlarged view of a) in the alkyl region between 0 and 3 ppm.

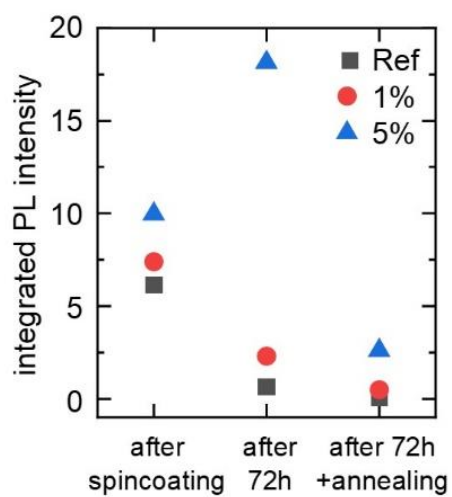


Fig S17: Alternative representation of Fig. 6c in the main text with absolute (integrated) values of the PL intensities.

S4: Details on the TRPL fittings

For fitting the TRPL data, we used the rate equation of the form⁴

$$\frac{dn}{dt} = -k_1n - k_2n^2 - k_3n^3, \quad (\text{S5})$$

where n is the (excess) charge carrier density after photoexcitation, and k_1 , k_2 , k_3 are the (defect related) monomolecular, (radiative) bimolecular and Auger recombination, respectively. $k_2 = 6.8 \times 10^{-10} \text{ cm}^3\text{s}^{-1}$ and $k_3 = 10^{-28} \text{ cm}^6\text{s}^{-1}$ were fixed as material parameters based on literature reports, and $n(t=0)$ was estimated as a starting value to be on the order of $5 \times 10^{16} \text{ cm}^{-3}$ based on the experimental conditions. Equation S5 was then solved numerically using the forward Euler algorithm with time steps of $\Delta t = 200 \text{ ps}$. From the decay of the charge carrier density, the (normalized) PL decay was calculated according to

$$I_{PL,fit}(t) \propto n(t)^2. \quad (\text{S6})$$

Equation S6 was then fitted to the experimental data using a least squares approach, where Equation S5 was solved in every iteration of the fitting procedure. k_1 and $n(t=0)$ were considered free parameters, resulting in k_1 values of $4.3 \times 10^7 \text{ s}^{-1}$, $7.2 \times 10^6 \text{ s}^{-1}$, $8.2 \times 10^6 \text{ s}^{-1}$ for the reference film and the films containing 1 mol% and 5 mol% IL, respectively. For $n(t=0)$, we obtain values of $2.1 \times 10^{17} \text{ cm}^{-3}$, $1.2 \times 10^{17} \text{ cm}^{-3}$, $1.4 \times 10^{17} \text{ cm}^{-3}$ for the reference film and the films containing 1 mol% and 5 mol% IL, agreeing well with the estimated initial value.

Supporting References

- 1K. Schötz, C. Greve, A. Langen, H. Gorter, I. Dogan, Y. Galagan, A. J. J. M. van Breemen, G. H. Gelinck, E. M. Herzig and F. Panzer, *Advanced Optical Materials*, 2021, **9**, 2101161.
- 2R. Munir, A. D. Sheikh, M. Abdelsamie, H. Hu, L. Yu, K. Zhao, T. Kim, O. E. Tall, R. Li, D.-M. Smilgies and A. Amassian, *Advanced Materials*, 2017, **29**, 1604113.
- 3J. C. Manificier, J. Gasiot and J. P. Fillard, *J. Phys. E: Sci. Instrum.*, 1976, **9**, 1002–1004.
- 4L. M. Herz, *Annual Review of Physical Chemistry*, 2016, **67**, 65–89.